Open Access Journal

Journal of Power Technologies 98 (1) (2018) 161–169

journal homepage:papers.itc.pw.edu.pl

Effect of hydrogen addition on the catalytic combustion of fuel-lean carbon monoxide-air mixtures over platinum for micro-scale power generation applications

Junjie Chen*, Longfei Yan, Wenya Song, Deguang Xu

School of Mechanical and Power Engineering, Henan Polytechnic University, Jiaozuo 454000, Henan, China

Abstract

The catalytic combustion of hydrogen and carbon monoxide over Pt/γ-Al_2O_3 catalyst was investigated numerically for H_2/CO/O_2/N_2 mixtures with overall lean equivalence ratios φ = 0.117 .. 0.167, H_2:CO molar ratios 1:1.5 .. 1:6, a pressure of 0.6 MPa, and a surface temperature range from 600 to 770 K relevant for micro-scale turbines and large gas turbine based power generation systems. Simulations were carried out with a two-dimensional CFD (Computational Fluid Dynamics) model in conjunction with detailed hetero-/homogeneous kinetic schemes and transports to explore the impact of hydrogen addition on catalytic combustion of carbon monoxide. The detailed reaction mechanisms were constructed by implementing recent updates to existing kinetic models. The simulation results indicated that the hydrogen addition kinetically promotes the catalytic combustion of carbon monoxide at wall temperatures as low as 600 K, whereby the catalytic reactions of hydrogen are fully lit-off and the conversion of carbon monoxide is mixed transport/kinetically controlled. Such a low temperature limit is of great interest to idling and part-load operation in large gas turbines and to normal operation for recuperative micro-scale turbine systems. Kinetic analysis demonstrated that the promoting impact of hydrogen addition on catalytic combustion of carbon monoxide is attributed to the indirect effect of hydrogen reactions on the surface species coverage, while direct coupling steps between hydrogen and carbon monoxide are of relatively minor importance. The added hydrogen inhibits the catalytic oxidation of carbon monoxide for wall temperatures below 520 K, which are well below the minimum inlet temperatures of reactants in micro-scale turbine based power generation systems.

Keywords: Catalytic combustion; Hydrogen promotion; Carbon monoxide; Synthesis gas; Power generation system

1. Introduction

The push toward the miniaturization of electromechanical devices and the resulting need for micro-scale power generation (milliwatts to watts) with long-life, low-weight devices has led to the recent development of the field of micro-scale combustion and power generation [1]. A miniaturized power-generating device, even with a relatively inefficient conversion of hydrocarbon fuels to power, would result in increased lifetime and/or reduced weight of an electronic or mechanical system that currently requires batteries for power [2]. Hydrocarbon fuels have energy densities much greater than the best batteries. Therefore, taking advantage of the high energy density of hydrocarbon fuels to generate power becomes an attractive technological alternative to batteries. To address the growing demand for smaller scale and higher energy density power sources, various combustion-based micro-scale power generators are being developed around the world. In addition, the availability of efficient micro-scale power generators will significantly enhance the functionality of power MEMS (Micro-Electro-Mechanical Systems) for many portable devices. Based on the high energy density of hydrocarbon fuels, a scale-down approach of existing large gas turbine for portable power sources has been conducted, and several micro-scale turbines have been developed [3–8], and sustainable combustion with high combustion efficiency for hydrocarbon fuels has been achieved in these millimeter-size gas turbines. Several micro-scale combustors have also been developed, and have been applied to energize thermoelectric systems to produce electrical power [9, 10]. Hydrogen-based micro-scale fuel cells have been successfully developed, and there is a need to develop reliable reformers (or direct-conversion fuel cells) for liquid hydrocarbons so that the fuel cells become competitive with batteries [11, 12].

The micro-scale power-generation devices (such as micro-scale turbines) addressed in the present work aim to

*Corresponding author
Email address: concjj@163.com (Junjie Chen)

generate power in the range of a few watts to milliwatts. This is in contrast to micro-turbines, which generate power of the order of kilowatts and are not “micro-scale” in the present sense. Power generation in the few-watts range has multiple applications, such as electronic devices (laptops, phones, etc.), extended duration applications of current devices, and miniaturized mechanical systems (small robots, rovers, airplanes, etc.). The corresponding combustion devices are of the order of millimeters in size [13]. Power generation in the milliwatt range has its application primarily in microelectronic components (sensors, transmitters, etc.). These micro-scale power-generation devices are constructed using primarily MEMS approaches and techniques [14].

There has been interest recently in syngas—produced through the gasification of coal or biomass which primarily contains hydrogen, carbon monoxide, carbon dioxide, and water—as an alternative fuel in power generation applications. Syngas is regarded as a promising alternative fuel of natural gas, for use in gas turbines [15, 16] and solid oxide fuel cells [17, 18]. The design of syngas-fueled turbines and combustors requires good knowledge of the combustion properties of syngas and hydrocarbon fuels [19–22]. In addition to large-scale power generation, syngas fuels are also attractive for micro-scale portable power generation [23]. In the presence of a catalyst, syngas can be produced from hydrocarbons in appropriate on-board microreformers [24–26]. Combustion in micro-scale power generations is typically accomplished in channels with hydraulic diameters ranging from less than one millimeter to a few millimeters [23]. The main combustible components in syngas are hydrogen and carbon monoxide, in addition to minimal amounts of methane and other hydrocarbons. Syngas combustion involves competitive oxidation reactions of hydrogen and carbon monoxide, which are very important for understanding other fuel processing technologies, such as partial oxidation of natural gas [27], water-gas shift [28], and preferential oxidation of carbon monoxide in excess hydrogen for cleaning hydrogen streams for fuel cell applications [29]. Moreover, the oxidation mechanisms of carbon monoxide and hydrogen are of fundamental importance as they are subsets of all hydrocarbon reaction mechanisms. It is well known that the oxidation of carbon monoxide requires traces of hydrogen-containing species. In the presence of a small amount of hydrogen or water, OH radicals are formed leading to the oxidation of carbon monoxide and to the production of H radicals, which feed into the chain-branching mechanism [23]. Furthermore, the application of combined hetero-/homogeneous combustion to syngas fuels is an attractive option for renewable and clean power generation, and can suppress most of the intrinsic flame instabilities appearing under non-catalytic (pure homogeneous combustion) conditions.

Due to the interest in syngas combustion in micro-scale turbines, recently there were numerous experimental and numerical studies devoted to improving the understanding of homogeneous kinetics of syngas fuels at elevated pressures [30]. However, there is a lack of corresponding high-pressure homogeneous and heterogeneous (catalytic) combustion investigations for hydrogen and carbon monoxide or syngas fuels in general. For syngas fuels, recent experimental and numerical investigations of hydrogen and carbon monoxide hetero-/homogenous combustion over platinum were performed at pressures of up to 5 and 15 bar to discover the kinetic and thermal effects [31, 32]. In a wider perspective, future utilization of syngas catalytic combustion relies on the development of active and stable catalysts as well as on the understanding of heterogeneous and homogeneous syngas kinetics under industrially-relevant operating conditions.

Note that all previous works referred to nearly isothermal reactor conditions, acquired either by heavily diluting the reactants to achieve very low exothermicity [33, 34] or by using high-thermal-conductivity foam catalysts (in the absence of large dilution) to rapidly equalize reactor temperature [30]. Given the highly sensitive impact of hydrogen addition on carbon monoxide, computations that entirely remove the requirement for reactor isothermicity, are highly desirable. In addition, in contrast to the well-known self-inhibition of carbon monoxide oxidation over platinum, the effects of hydrogen addition on the catalytic oxidation of carbon monoxide are still unclear. Hence, understanding the underlying heterogeneous hydrogen and carbon monoxide kinetics and their interactions over noble metal catalysts is crucial for the advancement of catalytic converters for emissions control and of syngas catalytic combustors for power generation.

The present work undertakes a numerical investigation of the catalytic combustion of syngas-air mixtures with various hydrogen and carbon monoxide compositions. Numerical predictions are carried out in typical catalytic combustor geometries at surface temperatures of 600 .. 770 K and pressure of 0.6 MPa. Such temperatures are of great interest for micro-scale turbine based power generation systems (inlet temperatures 600 .. 700 K for normal operation in recuperative micro-scale turbine systems [35, 36]) and for gas turbine combustors in large-scale power generation systems (inlet temperatures as low as 620 K at idling and part-load operation during synchronization with the network). $Pt/\gamma\text{-}Al_2O_3$ is the chosen catalyst because of its well-studied kinetics and its good reactivity for the oxidation of both hydrogen and carbon monoxide. Although metal oxides have been employed as catalysts for syngas combustion, their activity at the high pressures and narrow gaps encountered in power generation systems is not warranted. The main objectives of the present work are to identify the underlying kinetic processes which affect carbon monoxide oxidation in the presence of hydrogen, over temperature ranges where carbon monoxide oxidation is kinetically controlled.

It is within this context that the choice of fuels can be justified: while it is true that the syngas composition and relative amount of the constituents can vary widely due to the various types of feedstock used and also due to various methods of the gasification process, only hydrogen and carbon monoxide are chosen as fuels iso as to enable the chemical mechanisms responsible for the effect of hydrogen addition on the carbon monoxide oxidation to be identified. Since the

key purpose is to identify the underlying kinetic processes, this provides a useful perspective. In addition, micro-scale, simple geometries (such as micro-channels) are used in theoretical analysis and modeling mostly to focus on issues related to thermal behaviors and kinetic processes in particular in such configurations. Furthermore, simple geometrical configurations can be modeled accurately for the purposes of the detailed hetero-/homogeneous reaction mechanisms that will be discussed in the chemical kinetics section.

2. Numerical models and simulation approach

2.1. Geometric model

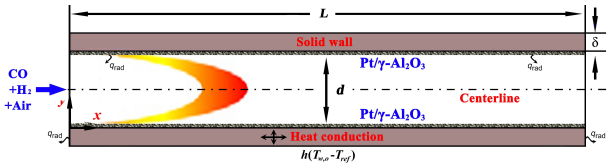

Figure 1: Schematic diagram of the catalytic channel-flow combustor.

A schematic diagram of the channel-flow combustor is illustrated in Fig. 1. It consists of two catalytically active parallel plates coated with Pt/γ-Al_2O_3 catalyst. Computations were performed for a steady laminar reactive flow in this catalytic combustor, simulating the 60.0 mm × 8.0 mm channel domain with the plate thickness δ = 2.0 mm, and resulting to confinements (surface-to-volume ratios) typical to those encountered in commercial catalytic combustors [37, 38]. The parallel plate geometry implies that the third dimension of this catalytic combustor is much larger than the gap size. Axial heat conduction in the solid is considered for a thermal conductivity k_s = 16.0 W/m K, corresponding to FeCr-alloy metallic honeycomb structures [38].

Additional properties needed in this model are the specific heat capacity and density of the FeCr-alloy solid, c_s = 700.0 J/kg K and ρ_s = 7220.0 kg/m^3, respectively. The fuel is syngas with varying hydrogen and carbon monoxide composition. The origin is fixed at the center of the inlet plane. In this work, x depicts the axial or downstream distance, and y represents the distance from the lower wall of two-dimensional parallel plates, respectively. Simulations were performed at 0.6 MPa with a range of CO/H_2 molar ratios and overall lean equivalence ratios 0.117 .. 0.167 (based on total fuels) in 30% vol. oxygen balanced by nitrogen.

The present work focuses on the effects of hydrogen addition on catalytic combustion of carbon monoxide, with pressure constant at 0.6 MPa. Nonetheless, 0.6 MPa is a suitable pressure for micro-scale turbine concepts [35, 36, 39].

2.2. Mathematical model

The characteristic length of the combustion chamber and the reacting gas flow path in catalytic channel-flow microcombustors is much larger than the molecular mean-free path of the air and other gases flowing through the system. Therefore, the fluid can be reasonably considered as continuous, and the Navier-Stokes equations are still applicable to the present work. The following assumptions were made: steady-state, gases follow the ideal gas law, the flow is laminar, and the pressure drop is negligible. With these assumptions, the governing equations were solved for a steady laminar reactive flow in two-dimensional catalytic combustors. CFD software, FLUENT® Release 6.3 [40] was used to perform these calculations. The laminar-finite-rate model was adopted to consider the interaction between flow and combustion. The governing equations for steady, laminar and reactive gas flow with hetero-/homogeneous reaction are shown below:

Continuity equation:

$$\frac{\partial(\rho v_x)}{\partial x} + \frac{\partial\left(\rho v_y\right)}{\partial y} = 0 \tag{1}$$

Momentum equation:

$$\frac{\partial\left(\rho v_x v_y\right)}{\partial x} + \frac{\partial\left(\rho v_x v_y\right)}{\partial y} = -\frac{\partial p}{\partial x} + \frac{\partial \tau_{xx}}{\partial x} + \frac{\partial \tau_{xy}}{\partial y} \tag{2}$$

$$\frac{\partial\left(\rho v_y v_x\right)}{\partial x} + \frac{\partial\left(\rho v_y v_y\right)}{\partial y} = -\frac{\partial p}{\partial y} + \frac{\partial \tau_{yx}}{\partial x} + \frac{\partial \tau_{yy}}{\partial y} \tag{3}$$

Energy equation:

$$\frac{\partial(\rho v_x h)}{\partial x} + \frac{\partial\left(\rho v_y h\right)}{\partial y} = \frac{\partial\left(k_f \partial T\right)}{\partial x^2} \tag{4}$$

$$+ \sum\left[\frac{\partial}{\partial x}\left(h_i \rho D_{i,m}\frac{\partial Y_i}{\partial y}\right) + \frac{\partial}{\partial y}\left(h_i \rho D_{i,m}\frac{\partial Y_i}{\partial y}\right)\right]$$

$$- \sum h_i R_i \tag{5}$$

Species equation:

$$\frac{\partial(\rho Y_i v_x)}{\partial x} + \frac{\partial\left(\rho Y_i v_y\right)}{\partial y} = -\left[\frac{\partial}{\partial x}\left(\rho D_{i,m}\frac{\partial Y_i}{\partial x}\right) + \frac{\partial}{\partial y}\left(\rho D_{i,m}\frac{\partial Y_i}{\partial y}\right)\right] + R_i \tag{6}$$

where ρ, v, p, τ and T denote the density, velocity, pressure, shear stress and temperature, respectively; h_i is the enthalpy of the ith species; k_f is the thermal conductivity of fluid; Y_i, R_i and D_{im} denote the mass fraction, the generation or consumption rate, and the mass diffusivity of the ith species.

Surface species coverage equations:

$$\frac{\partial \Theta_i}{\partial t} = \sigma_i \frac{s_i}{\Gamma}\left(i = N_g + 1, \ldots N_g + N_s\right) \tag{7}$$

where Θ_i, σ_i, and Γ denote the coverage and the molar production rate of the ith surface species, respectively. A surface site density Γ = 2.72 × 10^{-9} mol/cm^2 [38] is considered, simulating a polycrystalline Pt/γ-Al_2O_3 surface. N_g is the number of gas phase species and Ns is the number of

surface species. The left side of Eq. (7) is not a true transient term and was introduced only to facilitate convergence to steady state [41–43].

Since heat transfer along the wall significantly affects flame stability [44, 45], heat transfer along the wall was considered in this model. The appropriate energy equation for the solid phase is given as follows:

$$\frac{\partial\left(k_s \partial T\right)}{\partial x^2} + \frac{\partial\left(k_s \partial T\right)}{\partial y^2} = 0 \tag{8}$$

where k_s, W/m K, denotes the thermal conductivity of a solid wall.

2.3. Chemical kinetics

Heterogeneous kinetics was described with a detailed chemical reaction scheme from Deutschmann *et al.* [46] for hydrogen and carbon monoxide over Pt/γ-Al_2O_3, consisting of 24 reactions. This mechanism has reproduced catalytic ignition and steady combustion characteristics of hydrogen, carbon monoxide and methane fuels as well as mixtures of them [47, 48]. Seven gas phase species (H_2, CO, H_2O, CH_4, O_2, N_2, CO_2) are included in this mechanism, of which nitrogen is a chemically inert species. Eleven surface species (H(s), CO(s), C(s), O(s), OH(s), H_2O(s), CO_2(s), CH(s), CH_2(s), CH_3(s), Pt(s)) describe the coverage of the surface with adsorbed species. Methane reactions were not included as they were not relevant for the studied conditions. In addition, this scheme is augmented with HCOO(s) reactions of detailed surface reaction mechanism from Koop and Deutschmann [49]. The resulting syngas heterogeneous reaction mechanism consisted of 27 reactions among 8 surface species has been validated in works of Ghermay *et al.* [35, 50, 51] pure heterogeneous kinetic syngas studies. Furthermore, the formulation in Dogwiler *et al.* [52] with a modified Motz-Wise correction was employed for the adsorption rate constant kad,k of the kth gaseous species:

$$k_{ad,k} = \left(\frac{\gamma_k}{1 - \frac{\gamma_k \theta_{Pt}}{2}}\right) \frac{1}{\Gamma^m} \sqrt{\frac{RT}{2\pi W_k}} \tag{9}$$

where γ_k and W_k are the sticking coefficient and molecular weight of the kth gaseous species, respectively; θ_{Pt} is the Pt surface coverage; m is the sum of surface reactants' stoichiometric coefficients; R is the ideal gas constant; and T is the surface temperature.

The inclusion of gas-phase chemistry in catalytic combustion systems deserves special attention. For homogeneous chemistry, the mechanism of Li *et al.* [53] and Burke *et al.* [54] for hydrogen and carbon monoxide consisted of 36 reversible reactions involving 13 species was used with its accompanying gas-phase thermodynamic data. Reactions for carbon monoxide (R24-R36) were modeled with the elementary CO/HCO reaction subset in Li *et al.* [53] while hydrogen reactions (R1-R23) were taken from the latest H_2/O_2 kinetic model of Burke *et al.* [54]. This mechanism is only for the higher wall temperature cases, to verify the insignificance of gas-phase chemistry. This mechanism has been validated against flow reactor, shock tube, and laminar flame speed measurements at pressures of up to 87 bar.

Gas-phase and surface reaction rates were evaluated with CHEMKIN [55] and Surface-CHEMKIN [56], respectively. Mixture-average diffusion, including thermal diffusion for the light species, was used in conjunction with the CHEMKIN transport database [57].

2.4. Computation scheme

The boundary conditions used in this model are as follows. Uniform profiles for the axial velocity, the species concentrations and the temperature were specified at the inlet. At the exit, the pressure was specified and the remaining variables were calculated assuming far-field conditions, namely, zero diffusive flux of species or energy normal to the exit. A symmetry boundary condition was employed at the centerline between the two parallel plates. No slip was considered for either of the velocity components at the gas-wall interface; the heat flux at this gas-wall interface was calculated using Fourier's law along with continuity in temperature and heat flux was ensured. The two-dimensional energy equation was solved in the bulk of the wall. The radiation between the inner surfaces of the wall was considered using the discrete ordinates model [58]. The external surface of the wall, heat losses to the surroundings were calculated through Eq. (9), in which both natural convection and thermal radiation were considered.

$$q = h\left(T_{w,o} - T_{ref}\right) + \varepsilon\sigma\left(T_{w,o}^4 - T_{ref}^4\right) \tag{10}$$

where q is the heat flux, h is the external heat transfer coefficient, $T_{w,o}$ is the temperature at the external surface, ε is the emissivity of the solid surface, and σ is the Stephan-Boltzmann constant (5.67×10^{-8} W/(m^2 K^4)).

For the energy and species equations, Danckwerts boundary conditions were employed, i.e., the diffusive portions were calculated implicitly, and the convective portions of the equations were fixed. Non-uniform meshes were used with more grids distributed in the reaction region near the wall to provide sufficient grid resolution in the computational domain. Grid independence was examined and the final grid density was determined when the centerline profiles of temperature and species concentration did not show any obvious difference. The conservation equations were solved implicitly with the two-dimensional steady-state double-precision segregated solver using the under-relaxation method. The momentum, species, and energy equations were discretized using the second-order upwind scheme. The "SIMPLE" algorithm was used to couple the pressure and velocity. The fluid density was calculated using the ideal gas law. The fluid viscosity, thermal conductivity, and specific heat were calculated using the mass fraction weighted average of species properties. The species specific heat was calculated using the piecewise polynomial fit of temperature. The convergence of CFD simulation was judged based on the residuals of all governing equations. The simulation results were achieved with residuals smaller than 1.0×10^{-6}.

3. Results and discussion

Table 1: Updated reactions for catalytic combustion of hydrogen and carbon monoxide over Pt/γ-Al2O3 catalyst, only updated reactions are shown

γ (A)	n	Ea	Reactions
Adsorption and desorption reactions			
R1*		CO + Pt(s) → CO(s)	8
4×10^{-2}	0	0 0.0	
R2*		CO(s) → CO + Pt(s)	2
13×10^{13}	0	0 136,190-33,000$\theta_{CO(s)}$	
Surface reactions			
R3*		CO(s) + O(s) → CO_2(s) + Pt(s)	3
70×10^{20}	0	0 108,000-33,000$\theta_{CO(s)}$	
R4*		H(s) + O(s) → OH(s) + Pt(s)	3
70×10^{20}	0	0 70,500	
R5*		OH(s) + Pt(s) → H(s) + O(s)	1
00×10^{20}	0	0 130,690	
R6		OH(s) + CO(s) → HCOO(s) + Pt(s)	3
70×10^{21}	0	0 94,200	
R7		HCOO(s) + Pt(s) → OH(s) + CO(s)	1
33×10^{21}	0	0 870	
R8		HCOO(s) + O(s) → OH(s) + CO_2(s)	3
70×10^{21}	0	0 0.0	
R9		OH(s) + CO_2(s) → HCOO(s) + O(s)	2
79×10^{21}	0	0 151,050	
R10		HCOO(s) + Pt(s) → CO_2(s) + H(s)	3
70×10^{21}	0	0 0.0	
R11		CO_2(s) + H(s) → HCOO(s) + Pt(s)	2
79×10^{21}	0	0 90,050	

* Reactions are updated with kinetic data from Koop and Deutschmann [49]. R6-R11 are added HCOO reactions from Koop and Deutschmann [49]. R1 is given in terms of a sticking coefficient (γ) and is second order with respect to Pt(s). Units: γ; A, cm, s, K; Ea, J/mol; coverage θ. Surface site density $\Gamma = 2.7 \times 10^{-9}$ mol/cm^2.

Table 2: Simulation conditions

Case	φ	H_2, %vol.	CO, %vol.	T_{in}, K	u_{in}, m/s
A	0.167	4.0	6.0	300	2.0
B	0.150	3.0	6.0	300	2.0
C	0.133	2.0	6.0	300	2.0
D	0.117	1.0	6.0	300	2.0

Equivalence ratio: φ; inlet temperature: T_{in}; inlet velocity: u_{in} ; oxygen is 30% vol. with balance nitrogen.

Based on sensitivity and rate of production analyses, CO(s) oxidation and carbon monoxide adsorption/desorption reactions are essential components of the whole reaction scheme for carbon monoxide over platinum and they largely determined the kinetic model performance [20]. Therefore, kinetic parameters for the above key reactions and H(s) oxidation reaction were firstly updated in the scheme of Deutschmann *et al.* [46] according to recent literature data of Mhadeshwar *et al.* [29], and Koop and Deutschmann [49], then additional reactions involving the intermediate HCOO(s) [49] were added. The updated reactions for catalytic combustion of hydrogen and carbon monoxide over Pt/γ-Al_2O_3 catalyst are shown in Table 1 (only updated reactions are shown). Simulations were performed at 0.6 MPa with a range of CO/H_2 molar ratios and overall lean equivalence ratios 0.117-0.167 (based on total fuels) in 30% vol. oxygen balanced by nitrogen. Simulation conditions are shown in Table 2.

Fig. 2 shows the temperature contour for Case A. The reaction starts at the catalytic walls and a slow temperature

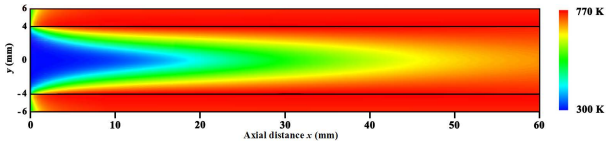

Figure 2: Temperature contours for Case A, u_{in} = 2.0 m/s, k_s = 16.0 W/m K, T_{in} = 300 K, and h = 20 W/(m^2 K)

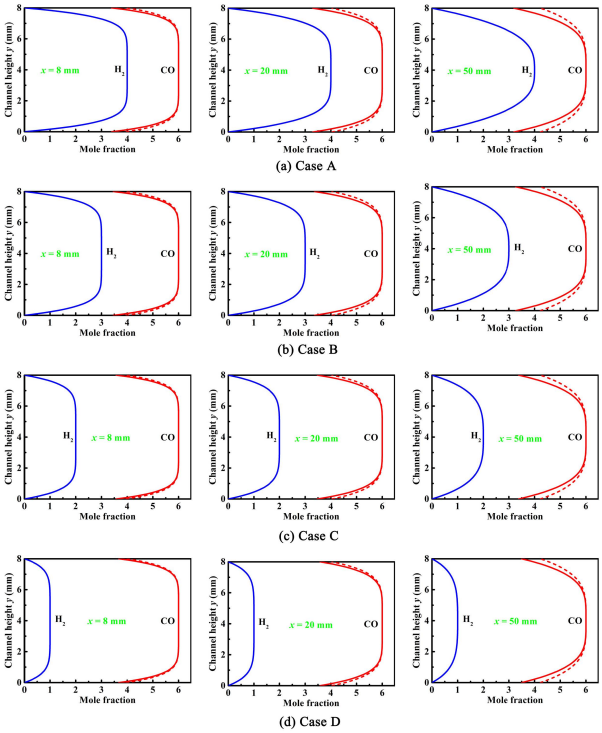

Figure 3: Transverse mole fraction profiles of carbon monoxide (red-lines) and hydrogen (blue-lines) for Cases A-D at three axial positions. Solid-lines and dashed-lines for carbon monoxide mole fractions are predictions of the kinetic model proposed herein and of the model without any hydrogen-involved reactions, respectively.

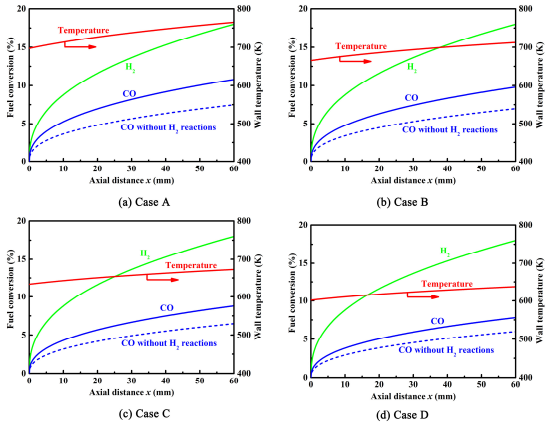

Figure 4: Hydrogen and carbon monoxide conversions and wall temperature profiles for Cases A-D. Red lines: wall temperature; green lines: hydrogen conversion from the kinetic scheme proposed herein; blue lines: carbon monoxide conversion from the full kinetic scheme, blue dotted-lines: carbon monoxide conversion from the kinetic scheme without hydrogen reactions.

rise is observed due to the exothermicity of the very lean fuel reaction. The wall acts as a net heat source due to axial recirculation, via wall conduction of the heat released by surface reaction. Simulated transverse profiles of hydrogen and carbon monoxide mole fractions are presented in Fig. 3 for Cases A-D. These cases have approximately the same carbon monoxide molar fraction (6% as shown in Table 2) and a hydrogen molar fraction dropping from 4.0% in Case A to 1.0% in Case D. The near-wall bending of species profiles represents that the hydrogen conversion is transport limited under the present temperatures, as demonstrated by the practically zero hydrogen concentration at both catalytic walls, while the carbon monoxide conversion exhibited finite-rate chemistry, i.e., mixed kinetically/transport-controlled. The examined temperatures (600 .. 770 K) of catalytic walls are of particular relevance to gas turbine combustors in large-scale power systems, with the lower values corresponding to inlet temperatures at idle operation during synchronization with the network. Moreover, species transport rates to catalytic walls are dictated by the flow Reynolds number which is kept approximately constant in all cases. Therefore, the hydrogen conversion is approximately the same, as also observed by the predicted profiles of hydrogen conversion in Fig. 4. In contrast, carbon monoxide conversion reflects the combined effects of transport and chemistry, and changes from approximately 10.8% in Case A to approximately 8.0% in Case D at the axial distance x = 60.0 mm. This variation is attributed to the decrease in catalytic wall temperatures from approximately 690 .. 770 K in Case A to approximately 600-680 K in Case D (as shown in Fig. 4), and to reduction of hydrogen content. The latter is of particular interest in this work.

Simulations were performed with hydrogen treated as an inert species by removing all hydrogen-relevant elementary reactions to delineate the kinetic effect of hydrogen addition on carbon monoxide, repeating the simulations for Cases A-D. The computing results compared to those of the full hydrogen and carbon monoxide reaction scheme are also shown in Fig. 3 and Fig. 4. It is evident that the presence of hydrogen promotes catalytic combustion of carbon monoxide for all cases. This promotion results in the enhancement of approximately 30 .. 44% local carbon monoxide conversion as shown in Fig. 4, which leads to further increases with increasing hydrogen content. Kinetic effects of hydrogen addition on carbon monoxide originated from two routes. One is directly via reactions involving surface species HCOO(s), as represented in Table 1. The formation and evolution of HCOO(s) provides an additional reaction route for carbon monoxide oxidation. The contribution from this direct coupling is estimated by repeating computations after eliminating all HCOO(s)-relevant elementary reactions. In this case, the results practically overlapped with those of the full hydrogen and carbon monoxide reaction scheme. The negligible contribution from the aforementioned direct pathway is because of the ultra-low branching ratio of the HCOO(s) formation elementary reaction CO(s) + OH(s) as compared with the oxidation elementary reaction CO(s) + O(s), as these two steps have similar reaction rate constants but, under the present conditions, OH(s) is several orders of magnitude lower than O(s).

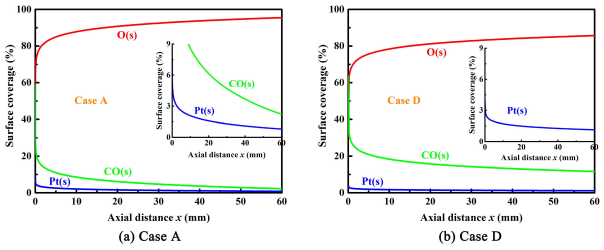

Figure 5: Surface coverage of Pt(s) and major species from the updated kinetic scheme for Cases A and D

The indirect way via surface species coverage is subsequently investigated due to the above direct coupling, but is minor. The consumption rate of carbon monoxide is largely dependent on the adsorption rate of carbon monoxide, which is in turn controlled by free Pt(s) active site availability. Hydrogen reactions increases the free Pt(s) active site and then promotes catalytic combustion of carbon monoxide. The reaction sequence is elaborated as follows: dissociative hydrogen adsorption to produce H(s), followed by H(s) oxidation reaction to OH(s) (R4 in Table 1) and further steps resulting in H_2O(s), which is finally desorbed to the gas phase. This route heavily consumes O(s) and releases free Pt(s) active site. The aforementioned analyses are supported by comparing variations of free Pt(s) active site. The computational results of Pt(s) coverage ratio are shown in Fig. 5 for Cases A and D, selected as they have the highest and the lowest surface temperatures, respectively. The surface coverage of major species for Cases A and D is also shown in Fig. 5. The enhanced Pt(s) coverage is significant in the presence of hydrogen reactions and varies with hydrogen composition. Richer hydrogen compositions impose stronger increase in Pt(s) coverage. Zheng *et al.* [31] demonstrated that wall temperatures significantly affect Pt(s) coverage. Furthermore, the lower temperatures renders this effect more pronounced, resulting in the smaller Pt(s) coverage.

Relevant inlet temperatures for large-scale power generations and for micro-scale turbine based power generation systems are in the range 600 .. 800 K. The lower temperature range 600 .. 700 K is of main interest for part-load and idling operation in large-scale gas turbines and for normal operation in recuperative micro-scale turbine systems. Therefore, for surface temperatures 600 .. 770 K encompassing the lowest inlet temperatures in large-scale gas turbines (idle operation) or the normal operating temperatures in recuperated micro-scale turbine systems, the addition of hydrogen to carbon monoxide promoted the catalytic combustion of the latter. These temperatures referred to partially light-off (mixed transport/kinetically controlled) carbon monoxide conversion and to fully light-off hydrogen reactions. This is actually expected to be the operational mode (part-load, idling and normal operation) in catalytic reactors of large gas turbines and micro-scale turbine systems, since

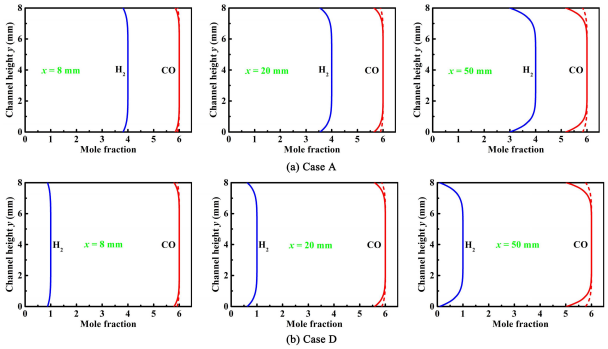

Figure 6: Transverse mole fraction profiles of carbon monoxide (red-lines) and hydrogen (blue-lines) for Cases A and D at constant surface temperature 500 K. Solid-lines and dashed-lines for carbon monoxide mole fractions are predictions of the kinetic model proposed herein and of the model without any hydrogen-involved reactions, respectively

the catalyst would attain the compressor discharge temperature (as low as 600 K) before fuel injection. Furthermore, simulations of all cases in Table 2 but with imposed constant wall temperatures 500 .. 600 K indicate that hydrogen addition started to inhibit the catalytic combustion of carbon monoxide only below 520 K. An example demonstrating this inhibition behavior is illustrated in Fig. 6, providing mole fraction profiles of hydrogen and carbon monoxide for Cases A and D but at the wall temperature of 500 K; therein, neither hydrogen or carbon monoxide is light-off, leading to very weak catalytic reactivity for both components as exhibited by their diminishing transverse concentration gradients at both catalytic walls. Operational temperatures below 520 K are clearly well-below the minimum inlet temperatures in small and large turbine-based power systems.

Another advantage of the adopted methodology is the use of a channel-reactor at realistic inlet Reynolds numbers for power generation systems, apart from the appropriate temperature range. Under such conditions, the hydrogen composition just above the Pt/γ-Al_2O_3 catalyst is, for practical power generation systems, very low because of transport limitations as demonstrated in Fig. 3. On the contrary, earlier isothermal reactor studies stated a complete lack of transport limitations. However, the effect of hydrogen addition on catalytic combustion of carbon monoxide is stronger in the absence of transport limitations. Simulations were performed using simplified low-dimensional models such as the surface perfectly stirred reactor (SPSR) [59, 60] at constant reactor temperatures 500 .. 700 K, surface-to-volume ratio 8 cm^{-1}, reactant compositions as in Table 2 and residence times of 8 .. 20 ms, relevant for power generation systems. Results indicated that the inhibition effect of hydrogen addition in the surface perfectly stirred reactor is demonstrated at higher temperatures of 540-560 K. This behavior is attributed to the large amounts of hydrogen available at the catalyst surface that competed with oxygen for adsorption, resulting in lower surface coverage for O(s) which is the deficient surface species controlling the oxidation rates.

4. Conclusion

The catalytic combustion of hydrogen and carbon monoxide over Pt/γ-Al_2O_3 catalyst was investigated numerically with a focus on surface temperatures 600 .. 770 K (a range of particular interest to idling and part-load operating conditions in either large-scale or small-scale power generation systems), fuel-lean total equivalence ratios 0.117 .. 0.167, H2:CO molar ratios 1:1.5 .. 1:6, and pressure of 0.6 MPa. Necessary updates were made to an existing kinetic scheme. In order to explore the impact of hydrogen addition on catalytic combustion of carbon monoxide, simulations were carried out with a two-dimensional CFD model in conjunction with elementary heterogeneous and homogeneous chemical reaction schemes, heat conduction in the solid wall, surface radiation heat transfer, and external heat losses. The following are the key conclusions of this study.

Hydrogen addition promoted the post-ignition stages of carbon monoxide oxidation at temperatures as low as 600 K, ranges pertaining to standard operational temperatures in recuperative micro-scale turbine systems or to idle operation in large gas turbine based power generation systems. This behavior is attributed to the hydrogen reaction routes, which effectively replenish deficient free Pt(s) active site, while the impact of direct coupling reactions between hydrogen and carbon monoxide via the intermediate HCOO(s) is negligible. Additional computations at lower temperatures referring to pre-ignition stages for both hydrogen and carbon monoxide were carried out, indicating that hydrogen addition inhibits catalytic oxidation of carbon monoxide. This behavior is attributed to the excess hydrogen available just above the Pt/γ-Al_2O_3 catalyst at the pre-ignition stages, which inhibits oxygen adsorption and consequently decreases the O(s) surface coverage that in turn controls the rate of CO(s) oxidation. Finally, the present study mainly focused on the effects of temperature on hydrogen-carbon monoxide interactions, while the pressure was constant at 0.6 MPa. Nonetheless, it is a suitable pressure for micro-scale turbine concepts; moreover, the higher pressures in large gas turbine based power generation systems might not significantly alter the findings with respect to hydrogen-carbon monoxide interactions because the oxidation of both hydrogen and carbon monoxide accelerates nearly proportionally with pressure.

Acknowledgments

This work was supported by the National Natural Science Foundation of China (No. 51506048).

References

[1] A. C. Fernandez-Pello, Micropower generation using combustion: Issues and approaches, Proceedings of the Combustion Institute 29 (1) (2002) 883–899.

[2] D. C. Walther, J. Ahn, Advances and challenges in the development of power-generation systems at small scales, Progress in Energy and Combustion Science 37 (5) (2011) 583–610.

[3] A. Mehra, X. Zhang, A. A. Ayón, I. A. Waitz, M. A. Schmidt, C. M. Spadaccini, A six-wafer combustion system for a silicon micro gas turbine engine, Journal of Microelectromechanical Systems 9 (4) (2000) 517–527.
[4] C. M. Spadaccini, J. Peck, I. A. Waitz, Catalytic combustion systems for microscale gas turbine engines, Journal of Engineering for Gas Turbines and Power 129 (1) (2005) 49–60.
[5] C. M. Spadaccini, A. Mehra, J. Lee, X. Zhang, S. Lukachko, I. A. Waitz, High power density silicon combustion systems for micro gas turbine engines, Journal of Engineering for Gas Turbines and Power 125 (3) (2003) 709–719.
[6] K. Isomura, M. Murayama, S. Teramoto, K. Hikichi, Y. Endo, S. Togo, S. Tanaka, Experimental verification of the feasibility of a 100 w class micro-scale gas turbine at an impeller diameter of 10 mm, Journal of Micromechanics and Microengineering 16 (9) (2006) 254–261.
[7] K. Isomura, S. Tanaka, S. Togo, H. Kanebako, M. Murayama, N. Saji, F. Sato, M. Esashi, Development of micromachine gas turbine for portable power generation, JSME International Journal Series B Fluids and Thermal Engineering 47 (3) (2004) 495–464.
[8] A. H. Epstein, micro-electro-mechanical systems gas turbine engines, Journal of Engineering for Gas Turbines and Power 126 (2) (2004) 205–226.
[9] T. Singh, R. Marsh, G. Min, Development and investigation of a non-catalytic self-aspirating meso-scale premixed burner integrated thermoelectric power generator, Energy Conversion and Management 117 (2016) 431–441.
[10] E. D. Tolmachoff, W. Allmon, C. M. Waits, Analysis of a high throughput n-dodecane fueled heterogeneous/homogeneous parallel plate microreactor for portable power conversion, Applied Energy 128 (2014) 111–118.
[11] Z. Zhang, W. Yuan, J. Deng, Y. Tang, Z. Li, K. Tang, Methanol catalytic micro-combustor with pervaporation-based methanol supply system, Chemical Engineering Journal 283 (2016) 982–991.
[12] C. H. Leu, S. C. King, J. M. Huang, C. C. Chen, S. S. Tzeng, C. I. Lee, W. C. Chang, C. C. Yang, Visible images of the catalytic combustion of methanol in a micro-channel reactor, Chemical Engineering Journal 226 (2013) 201–208.
[13] A. Brambilla, M. Schultze, C. E. Frouzakis, J. Mantzaras, R. Bombach, K. Boulouchos, An experimental and numerical investigation of premixed syngas combustion dynamics in mesoscale channels with controlled wall temperature profiles, Proceedings of the Combustion Institute 35 (3) (2015) 3429–3437.
[14] R. Sui, N. I. Prasianakis, J. Mantzaras, N. Mallya, J. Theile, D. Lagrange, M. Friess, An experimental and numerical investigation of the combustion and heat transfer characteristics of hydrogen-fueled catalytic microreactors, Chemical Engineering Science 141 (2016) 214–230.
[15] P. M. Allison, J. F. Driscoll, M. Ihme, Acoustic characterization of a partially-premixed gas turbine model combustor: Syngas and hydrocarbon fuel comparisons, Proceedings of the Combustion Institute 34 (2) (2013) 3145–3153.
[16] M. Gieras, T. Stankowski, Computational study of an aerodynamic flow through a micro-turbine engine combustor, Journal of Power Technologies 92 (2) (2012) 68–79.
[17] S. K. Aggarwal, D. Bongiovanni, M. Santarelli, Extinction of laminar diffusion flames burning the anodic syngas fuel from solid oxide fuel cell, International Journal of Hydrogen Energy 40 (22) (2015) 7214–7230.
[18] . Aydın, H. Nakajima, T. Kitahara, Current and temperature distributions in-situ acquired by electrode-segmentation along a microtubular solid oxide fuel cell operating with syngas, Journal of Power Sources 293 (2015) 1053–1061.
[19] Y. Zhang, W. Shen, H. Zhang, Y. Wu, J. Lu, Effects of inert dilution on the propagation and extinction of lean premixed syngas/air flames, Fuel 157 (2015) 115–121.
[20] W. Jerzak, M. Kuźnia, M. Zajemska, The effect of adding co2 to the axis of natural gas combustion flames on co and nox concentrations in the combustion chamber, Journal of Power Technologies 94 (3) (2014) 202–210.
[21] S. Morel, The afterburning of carbon monoxide in natural gas combustion gases in the presence of catalytic ceramic coatings, Journal of Power Technologies 92 (2) (2012) 109–114.
[22] A. Liu, B. Wang, W. Zeng, L. Chen, Experimental study of ch4 catalytic combustion on different catalyst, Journal of Power Technologies 93 (3) (2013) 142–148.
[23] A. Brambilla, C. E. Frouzakis, J. Mantzaras, R. Bombach, K. Boulouchos, Flame dynamics in lean premixed co/h2/air combustion in a mesoscale channel, Combustion and Flame 161 (5) (2014) 1268–1281.
[24] A. J. Santis-Alvarez, M. Nabavi, N. Hild, D. Poulikakos, W. J. Stark, A fast hybrid start-up process for thermally self-sustained catalytic n-butane reforming in micro-sofc power plants, Energy & Environmental Science 4 (8) (2011) 3041–3050.
[25] J. Thormann, L. Maier, P. Pfeifer, U. Kunz, O. Deutschmann, K. Schubert, Steam reforming of hexadecane over a rh/ceo2 catalyst in microchannels: Experimental and numerical investigation, International Journal of Hydrogen Energy 34 (12) (2009) 5108–5120.
[26] G. D. Stefanidis, D. G. Vlachos, N. S. Kaisare, M. Maestri, Methane steam reforming at microscales: Operation strategies for variable power output at millisecond contact times, AIChE Journal 55 (1) (2009) 180–191.
[27] A. B. Mhadeshwar, D. G. Vlachos, Hierarchical multiscale mechanism development for methane partial oxidation and reforming and for thermal decomposition of oxygenates on rh, The Journal of Physical Chemistry B 109 (35) (2005) 16819–16835.
[28] A. B. Mhadeshwar, D. G. Vlachos, Is the water-gas shift reaction on pt simple?: Computer-aided microkinetic model reduction, lumped rate expression, and rate-determining step, Catalysis Today 105 (1) (2005) 162–172.
[29] A. B. Mhadeshwar, D. G. Vlachos, Microkinetic modeling for water-promoted co oxidation, water-gas shift, and preferential oxidation of co on pt, The Journal of Physical Chemistry B 108 (39) (2004) 15246–15258.
[30] M. Schultze, J. Mantzaras, F. Grygier, R. Bombach, Hetero-/homogeneous combustion of syngas mixtures over platinum at fuel-rich stoichiometries and pressures up to 14 bar, Proceedings of the Combustion Institute 35 (2) (2015) 2223–2231.
[31] X. Zheng, J. Mantzaras, R. Bombach, Kinetic interactions between hydrogen and carbon monoxide oxidation over platinum, Combustion and Flame 161 (1) (2014) 332–346.
[32] J. Mantzaras, Catalytic combustion of syngas, Combustion Science and Technology 180 (6) (2008) 1137–1168.
[33] M. Sun, E. B. Croiset, R. R. Hudgins, P. L. Silveston, M. Menzinger, Steady-state multiplicity and superadiabatic extinction waves in the oxidation of co/h2 mixtures over a pt/al2o3-coated monolith, Industrial & Engineering Chemistry Research 42 (1) (2003) 37–45.
[34] J. A. Federici, D. G. Vlachos, Experimental studies on syngas catalytic combustion on pt/al2o3 in a microreactor, Combustion and Flame 158 (12) (2011) 2540–2543.
[35] Y. Ghermay, J. Mantzaras, R. Bombach, Experimental and numerical investigation of hetero-/homogeneous combustion of co/h2/o2/n2 mixtures over platinum at pressures up to 5 bar, Proceedings of the Combustion Institute 33 (2) (2011) 1827–1835.
[36] S. Eriksson, M. Wolf, A. Schneider, J. Mantzaras, F. Raimondi, M. Boutonnet, S. Järås, Fuel-rich catalytic combustion of methane in zero emissions power generation processes, Catalysis Today 117 (4) (2006) 447–453.
[37] S. Eriksson, A. Schneider, J. Mantzaras, M. Wolf, S. JärÅs, Experimental and numerical investigation of supported rhodium catalysts for partial oxidation of methane in exhaust gas diluted reaction mixtures, Chemical Engineering Science 62 (15) (2007) 3991–4011.
[38] A. Schneider, J. Mantzaras, P. Jansohn, Experimental and numerical investigation of the catalytic partial oxidation of ch4/o2 mixtures diluted with h2o and co2 in a short contact time reactor, Chemical Engineering Science 61 (14) (2006) 4634–4649.
[39] J. Duan, L. Sun, G. Wang, F. Wu, Nonlinear modeling of regenerative cycle micro gas turbine, Energy 91 (2015) 168–175.
[40] FLUENT, Fluent 6.3 user's guide, Tech. rep., Fluent Inc., Lebanon, New Hampshire, USA (2006).
[41] J. Mantzaras, C. Appel, P. Benz, U. Dogwiler, Numerical modelling of turbulent catalytically stabilized channel flow combustion, Catalysis Today 59 (1-2) (2000) 3–17.

[42] J. Mantzaras, P. Benz, An asymptotic and numerical investigation of homogeneous ignition in catalytically stabilized channel flow combustion, Combustion and Flame 119 (4) (1999) 455–472.
[43] J. Mantzaras, C. Appel, Effects of finite rate heterogeneous kinetics on homogeneous ignition in catalytically stabilized channel flow combustion, Combustion and Flame 130 (4) (2002) 336–351.
[44] D. G. Norton, D. G. Vlachos, Combustion characteristics and flame stability at the microscale: a cfd study of premixed methane/air mixtures, Chemical Engineering Science 58 (21) (2003) 4871–4882.
[45] D. G. Norton, D. G. Vlachos, A cfd study of propane/air microflame stability, Combustion and Flame 138 (1-2) (2004) 97–107.
[46] O. Deutschmann, L. Maier, U. Riedel, A. H. Stroeman, R. W. Dibble, Hydrogen assisted catalytic combustion of methane on platinum, Catalysis Today 59 (1-2) (2000) 141–150.
[47] C. Appel, J. Mantzaras, R. Schaeren, R. Bombach, A. Inauen, B. Kaeppeli, B. Hemmerling, A. Stampanoni, An experimental and numerical investigation of homogeneous ignition in catalytically stabilized combustion of hydrogen/air mixtures over platinum, Combustion and Flame 128 (4) (2002) 340–368.
[48] M. Schultze, J. Mantzaras, Hetero-/homogeneous combustion of hydrogen/air mixtures over platinum: Fuel-lean versus fuel-rich combustion modes, International Journal of Hydrogen Energy 38 (25) (2013) 10654–10670.
[49] J. Koop, O. Deutschmann, Detailed surface reaction mechanism for pt-catalyzed abatement of automotive exhaust gases, Applied Catalysis B: Environmental 91 (1-2) (2009) 47–58.
[50] Y. Ghermay, J. Mantzaras, R. Bombach, Effects of hydrogen preconversion on the homogeneous ignition of fuel-lean h2/o2/n2/co2 mixtures over platinum at moderate pressures, Combustion and Flame 157 (10) (2010) 1942–1958.
[51] Y. Ghermay, J. Mantzaras, R. Bombach, K. Boulouchos, Homogeneous combustion of fuel-lean h2/o2/n2 mixtures over platinum at elevated pressures and preheats, Combustion and Flame 158 (8) (2011) 1491–1506.
[52] U. Dogwiler, P. Benz, J. Mantzaras, Two-dimensional modelling for catalytically stabilized combustion of a lean methane-air mixture with elementary homogeneous and heterogeneous chemical reactions, Combustion and Flame 116 (1-2) (1999) 243–258.
[53] J. Li, Z. Zhao, A. Kazakov, M. Chaos, F. L. Dryer, J. J. S. Jr., A comprehensive kinetic mechanism for co, ch2o, and ch3oh combustion, International Journal of Chemical Kinetics 39 (3) (2007) 109–136.
[54] M. P. Burke, M. Chaos, Y. Ju, F. L. Dryer, S. J. Klippenstein, Comprehensive h2/o2 kinetic model for high-pressure combustion, International Journal of Chemical Kinetics 44 (7) (2012) 444–474.
[55] R. J. Kee, F. M. Rupley, E. Meeks, J. A. Miller, Chemkin-iii: A fortran chemical kinetics package for the analysis of gas-phase chemical and plasma kinetics, Tech. Rep. Report No. SAND96-8216, Sandia National Laboratories, Livermore, CA (USA) (1996).
[56] M. E. Coltrin, R. J. Kee, F. M. Rupley, E. Meeks, Surface chemkin-iii: A fortran package for analyzing heterogeneous chemical kinetics at a solid-surface - gas-phase interface, Tech. Rep. Report No. SAND96-8217, Sandia National Laboratories, Livermore, CA (USA) (1996).
[57] R. J. Kee, G. Dixon-Lewis, J. Warnatz, M. E. Coltrin, J. A. Miller, H. K. Moffat, A fortran computer code package for the evaluation of gas-phase, multicomponent transport properties, Tech. Rep. Report No. SAND86-8246B, Sandia National Laboratories, Livermore, CA (USA) (1998).
[58] C. H. Kuo, P. D. Ronney, Numerical modeling of non-adiabatic heat-recirculating combustors, Proceedings of the Combustion Institute 31 (2) (2007) 3277–3284.
[59] A. K. Chaniotis, D. Poulikakos, Modeling and optimization of catalytic partial oxidation methane reforming for fuel cells, Journal of Power Sources 142 (1-2) (2005) 184–193.
[60] E. Meeks, H. K. Moffat, J. F. Grcar, R. J. Kee, Aurora: A fortran program for modeling well stirred plasma and thermal reactors with gas and surface reactions, Tech. Rep. Report No. SAND96-8218, Sandia National Laboratories, Livermore, CA (USA) (1996).